Microemulsion Polymerization. 1. Small-Angle Neutron Scattering Study of Monomer Partitioning

Carlos C. Co, Renko de Vries, and Eric W. Kaler*

Center for Molecular and Engineering Thermodynamics, Department of Chemical Engineering, University of Delaware, Newark, Delaware 19716

Received July 18, 2000; Revised Manuscript Received January 2, 2001

ABSTRACT: To achieve a better understanding of the kinetics of microemulsion polymerization, we have examined monomer partitioning between micelles and polymer particles during polymerization of aqueous microemulsions of dodecyltrimethylammonium bromide surfactant and styrene, *n*-butyl methacrylate, *tert*-butyl methacrylate, and *n*-hexyl methacrylate monomers. Polymerizing microemulsions are simulated by equilibrium mixtures of unpolymerized and fully polymerized microemulsions for which the monomer partitioning is accurately measured using small-angle neutron scattering. Experimental results are semiquantitatively reproduced by modeling the monomer partitioning as a competition between the Flory−Huggins bulk polymer free energy and the Helfrich curvature elastic energy of the surfactant monolayers.

1. Introduction

Microemulsion polymerization is a convenient process for the production of ultrafine latex particles (10−50 nm) consisting of very high molecular weight polymers (∼15 × 10^6 Da) that are difficult to prepare using conventional emulsion polymerization processes. In view of the many potential applications of small latex particles and very high molecular weight polymers, it is important to be able to predict and control the kinetics, particle size, and molecular weight distributions of these latexes. In this three part series, we have investigated in detail the partitioning of monomer between micelles and polymer particles (part 1) and its effect together with biradical termination and glass transition on the polymerization kinetics (part 2) as well as the molecular weight and particle size distributions (part 3). These studies focus on the batch polymerizations of simple model microemulsions to facilitate the interpretation of experimental results. Nevertheless, the mechanistic insights gleaned from these studies can be extended to more efficient microemulsions or the operation of semibatch microemulsion polymerization processes where the final polymer volume fraction in the latexes can exceed 30%.[1,2] A detailed mechanistic understanding of polymerization in these microemulsions consisting of simple droplet microstructures may also be useful in developing a better understanding of the general aspects of other polymerizations in surfactant solutions such as the polymerization of hydrophobic monomers in vesicles,[3] bicontinuous phases, and liquid crystalline phases.[4−6]

While the formation of ultrafine latex particles during microemulsion polymerization has been studied by many authors since the 1980s as reviewed by Antonietti et al.,[7] there have only been a few attempts at modeling the reaction kinetics[8−12] or molecular weight and particle size distributions.[12,13] Previously, we have developed a simple model[10] for the kinetics of microemulsion polymerization that is based on the assumptions that bimolecular termination is negligible and that the monomer concentration $C_{mon}^{(part)}$ in the growing particles is proportional to the amount of unreacted monomer,

$$C_{mon}^{(part)} \propto 1 - f \tag{1}$$

where f is the fractional conversion of the polymerization reaction. With these assumptions, a rate maximum is predicted to occur at a conversion of $1 - e^{-1/2}$ or 39%, irrespective of any characteristic of the system. For the polymerization of *n*-hexyl methacrylate (C_6MA) in mixed microemulsions of the cationic surfactants dodecyltrimethylammonium bromide (DTAB) and didodecyldimethylammonium bromide (DDAB), the rate maximum indeed occurs at around 39%. For this system, the simple model quantitatively predicts the kinetics without adjustable parameters. Rate maxima at ∼40% conversion has also been reported by Capek and Juranicova[14] for the microemulsion polymerizations of ethylhexyl methacrylate. Reanalysis of the kinetic data by Full et al.[15] for tetrahydrofurfuryl methacrylate microemulsions once again reveal a rate maximum at ∼40% conversion. Note that in both cases the monomers have very low water solubilities and low polymer glass transition temperatures. However, all other systems that have been studied so far seem to have rate maxima at conversions significantly below 40%. Indeed, essentially the same model was later rederived by Nomura et al.[11,12] to account for the kinetics of styrene microemulsion polymerization initiated with water-soluble initiators that typically exhibit a rate maximum at ∼20% conversion. The authors concluded that the model was inconsistent with the observed kinetics for styrene, except at low conversions. More recently, they suggested nonlinear monomer partitioning as a probable cause for the discrepancies.[12]

The aim of the present series of papers is to understand why the simple theory fails and to extend it to account for the kinetics of other systems. The first step is to take a closer look at the fundamental assumptions underlying the simple theory, using both theoretical and experimental observations. The kinetics of the polymerization reactions and particle size and molecular weight distributions are considered in parts 2 and 3 of this series.

* Corresponding author. Tel (302) 831-3553; Fax (302) 831-8201; E-mail kaler@che.udel.edu.

10.1021/ma001246r CCC: $20.00
Published on Web 04/05/2001

Here the factors that determine the monomer concentration in the growing polymer particles during the polymerization reaction are examined. The fundamental point is that, in a polymerizing microemulsion, polymer particles coexist with a large excess of surfactant micelles throughout the reaction, and the two species compete for the unreacted monomer. The monomer concentration in the growing polymer particles is determined by how the monomer partitions between the polymer particles and the surfactant micelles. Since monomer exchange is fast on the time scale of the polymerization reaction, monomer partitioning is governed by equilibrium thermodynamics. The rate of polymerization is directly proportional to the concentration of monomer in the growing polymer particles. Therefore, the partitioning of monomer provides the key connection between the polymerization kinetics and the microemulsion thermodynamics and hence then to microemulsion microstructure and phase behavior.

Two limiting cases can be identified with respect to monomer partitioning: (1) the monomer resides mainly in the micelles and does not swell the particles, and (2) the monomer extensively swells the particles, and the micelles are depleted of monomer very early on in the reaction. The first limiting case, it is argued,[10,13,16] applies to the C_6MA/DTAB/DDAB microemulsion polymerizations. Polymerization is assumed to occur in the monomer-swollen hydrocarbon chains of the surfactant molecules adsorbed on the particles. This hypothesis, together with an analytical theory[13] for the evolution of the particle size distribution during microemulsion polymerization, led to model small-angle neutron-scattering (SANS) spectra that were in quantitative agreement with on-line SANS spectra of polymerizing C_6MA/DTAB/DDAB microemulsions.[16] On the other hand, on the basis of a thermodynamic model, Guo et al.[17] have argued that for styrene microemulsion polymerization the second limiting case applies. Both the Morgan et al.[10] hypothesis and the model of Guo et al.[17] lead to a monomer partitioning profile that is essentially linear, as expressed by eq 1.

As yet there are no independent measurements of the monomer concentration in the polymer particles during microemulsion polymerization, and so there is no validation of the fundamental hypothesis of linear monomer partitioning, eq 1. Further progress in modeling the polymerization kinetics clearly requires such measurements. So far, the only independent measurement of the monomer concentration in polymer particles during microemulsion polymerization are due to Manders et al.[18] Using a pulsed laser polymerization (PLP) technique, these authors demonstrate that, for styrene microemulsion polymerization at low conversions, the monomer concentration in the polymer particles increases with increasing monomer content of the initial microemulsion. Unfortunately, the PLP technique is restricted to low conversions, so it cannot be used to test eq 1 fully.

Since it is impossible to separate the monomer-swollen polymer particles from the monomer-swollen micelles without affecting the swelling equilibrium, traditional determinations of monomer swelling[19] are not applicable. Instead, a technique is needed that can distinguish between the swelling of micelles and particles in mixtures containing both of them. Quasi-elastic light scattering (QLS) has been used by some researchers to estimate the swelling of polymer particles. However, accurate particle size measurements are possible only when multiple scattering effects and interparticle interactions can be ignored. In general, diluted samples are necessary to satisfy these requirements. Our attempts to measure monomer partitioning using QLS indicated that the swelling equilibrium strongly depends on the concentration of both polymer particles and surfactant. These experimental issues severely limit the accuracy of monomer partitioning results acquired using QLS. In contrast, properly analyzed small-angle neutron scattering (SANS) measurements can reveal the sizes of both particles and micelles without dilution.

The goal of this paper is to test eq 1 and to relate the measured monomer partitioning, and hence the polymerization kinetics, to the microemulsion microstructure and phase behavior. To interpret these results, a new thermodynamic model is developed for monomer partitioning during microemulsion polymerization.

Cationic DTAB microemulsions made with a range of hydrophobic monomers—styrene, *n*-butyl methacrylate (nC_4MA), *tert*-butyl methacrylate (tC_4MA), and C_6MA—are studied. For all cases the linear profile (eq 1) provides a fair description of the monomer partitioning. Deviations from linearity appear to be related to the location of the microemulsion composition in the phase diagram, and they are largest for microemulsion compositions close to phase separation. Furthermore, at constant surfactant concentration, the monomer concentration in the polymer particles increases with increasing monomer content of the initial microemulsions, consistent with the low conversion results of Manders et al.[18]

These observations can be explained in terms of a simple thermodynamic model. Particle swelling is favored by the bulk polymer free energy, which is described by the Flory−Huggins expression. Swelling is opposed by the Helfrich[20] curvature elastic energy of the surfactant monolayers of the microemulsion droplets, which promotes their swelling with monomer until they reach their preferred or "spontaneous" curvature. Microemulsion phase behavior is governed to a large extent by the curvature elastic properties of surfactant monolayers, especially by their spontaneous curvature.[21] Hence, the curvature elastic properties of the surfactant monolayer as incorporated in our monomer partitioning model connect the microemulsion phase behavior and microstructure to the monomer concentration in the particles and, ultimately, to the polymerization kinetics. The monomer-partitioning model correctly predicts both the deviations from linear monomer partitioning for microemulsion compositions close to the phase boundary and the trend of increasing monomer concentration in the particles for microemulsions with increasing monomer content.

2. Materials and Methods

DTAB from TCI America with 99+% purity was used as received. Styrene, nC_4MA, tC_4MA, and C_6MA (Scientific Polymer Products, 99%) were vacuum distilled and stored below 0 °C for less than 5 days before use. The initiator, 2,2′-azobis(2-amidinopropane) hydrochloride (V50) (Wako Pure Chemical Industries, Ltd., 98.8%), and D_2O (Cambridge Isotopes Laboratories, 99.9%, low conductivity) were used as received.

Microemulsions of styrene, nC_4MA, tC_4MA, and C_6MA containing 12 wt % DTAB and 2.64 wt % of nitrogen sparged monomer in degassed D_2O were prepared in 40 mL vials inside a glovebag purged five times with nitrogen. Following a

common notation, compositions in weight percentages are reported as α = oil/(oil + water) × 100 and γ = surfactant/(surfactant + oil + water) × 100; this microemulsion corresponds to α = 3% and γ = 12%. After removal from the glovebag, the headspace of the vials was thoroughly purged with ultrahigh-purity nitrogen. To polymerize these microemulsions, the samples were heated to 60 °C and initiated by injecting 0.5 mL of a degassed D_2O solution containing 0.063 wt % of V50 with respect to the amount of monomer in the microemulsion to give an overall concentration of 1.1×10^{-4} M. The samples were allowed to polymerize for 6 h at 60 °C. Gravimetric analysis showed that respectively 92%, 100%, 92%, and 100% of the styrene, nC_4MA, tC_4MA, and C_6MA had been polymerized. To thoroughly decompose the residual V50 initiator (10 min half-life at 90 °C), the samples were heated at 90 °C in an oven for 24 h. After this heat treatment, the styrene conversion increased to 96% and the t-C4MA conversion to 97%. A separate polymerized styrene microemulsion containing 6.6 wt % of monomer (α = 7.5%) was prepared in the same way for the styrene SANS swelling studies performed at α = 5% and 7.5%.

For the equilibrium SANS swelling experiments, samples containing varying ratios of the polymerized microemulsions and original unpolymerized microemulsions were mixed in vials and transferred into 2 mm path length SANS cells. The SANS cells were made from stainless steel blocks with crystalline quartz windows sealed with Teflon-coated silicone O-rings. The samples were allowed to equilibriate at 60 °C before SANS spectra were acquired. No sample evaporation could be detected from a cell containing unpolymerized styrene microemulsion even after 12 h at 80 °C.

For the online SANS experiments, the polymerizations were carried out in a 500 mL reactor located adjacent to the neutron beam. The contents of the reactor were flowed periodically into 2 mm path length SANS cells thermostated at 60 °C that were then transferred manually into the neutron beam. During the initial stages of reaction when the polymerization rate is high, SANS spectra were acquired every 90 s. Immediately before and after each SANS sample, ~4 mL aliquots were removed and analyzed gravimetrically for conversion to an accuracy of ±1%. Exposure of the polymerizing microemulsion to atmospheric oxygen as it flows from the reactor quenches the reaction instantaneously.

Both equilibrium and online SANS experiments were performed on the NG7 spectrometer at the Cold Neutron Research Facility of the National Institute of Standards and Technology (NIST). The neutron wavelength was $\lambda = 6$ Å with $\Delta\lambda/\lambda = 0.15$. All scattering spectra were corrected for background, detector sensitivity, empty cell scattering, and sample transmission. The spectra were then radially averaged and placed on an absolute scale through direct calibration of the beam flux.

3. Thermodynamics of Monomer Partitioning

This section introduces a simple thermodynamic model for monomer partitioning during microemulsion polymerization. Provided the establishment of a thermodynamic swelling equilibrium is much faster than the monomer consumption of the polymerization reaction, the monomer partitioning can be described by equilibrium thermodynamics. This is known to be a reasonable approximation for emulsion polymerization,[19] except at high conversions where the polymer may become glassy. In view of the very small particle sizes produced, the approximation is expected to be even better for microemulsion polymerization. Hence, the partitioning is assumed to be described by equilibrium thermodynamics:

$$\mu_{\text{mon}}^{(\text{mic})} = \mu_{\text{mon}}^{(\text{part})} \tag{2}$$

where $\mu_{\text{mon}}^{(\text{mic})}$ and $\mu_{\text{mon}}^{(\text{part})}$ are the monomer chemical potentials in the swollen micelles (or microemulsion droplets) and in the polymer particles, respectively. The composition of the initial microemulsion is set by the initial volume fraction of monomer ($\phi_{\text{mon},0}$) and the volume fraction of surfactant (ϕ_{surf}). Neglecting small changes in volume upon polymerization, the total monomer and polymer volume fractions during the reaction are given by

$$\phi_{\text{mon}} = (1 - f)\phi_{\text{mon},0} \tag{3}$$

$$\phi_{\text{pol}} = f\phi_{\text{mon},0} \tag{4}$$

where f is the fractional conversion of monomer into polymer. The monomer partitions between the micelles and the particles:

$$\phi_{\text{mon}} = \phi_{\text{mon}}^{(\text{mic})} + \phi_{\text{mon}}^{(\text{part})} \tag{5}$$

Typically, only a small fraction of the surfactant adsorbs on the particles. This fraction is neglected in calculating the extent of swelling of the micelles, as is any variation of the surfactant headgroup area. A convenient parameter characterizing the swelling of the micelles is thus

$$x \equiv \frac{R_{\text{mic}}}{R_{\text{mic},0}} = 1 + \frac{\phi_{\text{mon}}^{(\text{mic})}}{\phi_{\text{surf}}} \tag{6}$$

where R_{mic} is the radius of the micelles and $R_{\text{mic},0}$ is the radius of the empty micelles. The volume fraction of monomer in the polymer particles characterizes the extent of swelling of the particles:

$$\nu_{\text{mon}} = \frac{\phi_{\text{mon}}^{(\text{part})}}{\phi_{\text{pol}} + \phi_{\text{mon}}^{(\text{part})}} \tag{7}$$

Neglecting the small contribution of the adsorbed surfactant layer to the total volume of the particles, the two parameters are related by the following mass balance:

$$x = 1 + \frac{\phi_{\text{mon},0}}{\phi_{\text{surf}}}\left(1 - \frac{f}{1 - \nu_{\text{mon}}}\right) \tag{8}$$

3.1. Monomer Chemical Potential in the Micelles. Using the Helfrich expression[20] as an approximation to the curvature elastic energy of the surfactant monolayers, the curvature elastic energy of a spherical microemulsion droplet or swollen micelle with radius R_{mic} can be expressed as

$$F_{\text{curv}} = 4\pi(2k_c + \bar{k}_c) - 8\pi k_c c_0 R_{\text{min}} \tag{9}$$

The spontaneous curvature (c_0), the bending modulus (k_c), and the modulus of Gaussian curvature ($\bar{k}_c$) include contributions due to the electric double layers that surround the microemulsion droplets.[22−25] A smaller contribution to the free energy per microemulsion droplet is due to the droplet translational entropy. This contribution is approximated by

$$\frac{F_{\text{trans}}}{k_B T} = \ln \phi + c_{\text{trans}} \tag{10}$$

where $\phi \equiv \phi_{\text{mon}}^{(\text{mic})} + \phi_{\text{surf}}$ is the total volume fraction of microemulsion droplets. The numerical constant c_{trans}

is of order one. It is related to the length scale over which a microemulsion droplet should be translated in order to be counted as a new configuration, an issue that is still under debate.[26−28] The number density of microemulsion droplets is

$$\rho_{mic} = \frac{\phi}{\frac{4}{3}\pi R_{mic}^3} = \frac{\phi_{surf}}{\frac{4}{3}\pi R_{mic,0}^3}\frac{1}{x^2} \tag{11}$$

so the free energy density of the microemulsion can be expressed as

$$f_{mic} = \rho_{mic}(F_{curv} + F_{trans}) \tag{12}$$

and the monomer chemical potential in the micelles is

$$\frac{\mu_{mon}^{(mic)}}{V_{mon}} = \frac{\partial f_{mic}}{\partial \phi_{mon}^{(mic)}} = -\frac{6}{R_{mic}^3}\left\{(2k_c + \bar{k}_c) - k_c c_0 R_{mic} + k_B T \frac{\ln \phi + c_{entr} - \frac{1}{2}}{4\pi}\right\} \tag{13}$$

where V_{mon} is the volume of a monomer molecule. The maximum amount of monomer $\phi_{mon,max}$ that can be solubilized in the micelles or microemulsion droplets, or, equivalently, the phase boundary, is found by setting $\mu_{mon}^{(mic)} = 0$. In this case

$$k_c c_0 R_{mic,max} = (2k_c + \bar{k}_c) - k_B T \frac{\ln(\phi_{surf} + \phi_{mon,max}) + c_{entr} - \frac{1}{2}}{4\pi} \tag{14}$$

where $R_{mic,max} = R_{mic,0}(1 + \phi_{mon,max}/\phi_{surf})$ is the corresponding maximum radius of the swollen micelles. In terms of this experimentally accessible quantity, the expression for the monomer chemical potential in the micelles can be rewritten as

$$\mu_{mon}^{(mic)} = -\frac{6V_{mon}}{R_{mic}^3}\left\{k_c c_0(R_{mic,max} - R_{mic}) + \frac{k_B T}{4\pi}\ln(R_{mic}/R_{mic,max})\right\} \tag{15}$$

This clearly shows how the monomer chemical potential in the micelles at a given composition depends on the distance to the phase boundary.

3.2. Monomer Chemical Potential in the Polymer Particles. The monomer chemical potential in the polymer particles has contributions due to both the polymer and the adsorbed layers of surfactant on the particles. The latter contribution is small and will be neglected. The polymer contribution consists of a bulk term $\mu_{mon}^{(part,b)}$ and a surface term $\mu_{mon}^{(part,s)}$. The high molecular weight Flory−Huggins expression describes the bulk polymer contribution:

$$\frac{\mu_{mon}^{(part,b)}}{k_B T} = \ln(1 - \nu_{pol}) + \nu_{pol} + \chi \nu_{pol}^2 \tag{16}$$

where $\nu_{pol} = 1 - \nu_{mon}$ is the volume fraction of polymer in the particles. Interactions between polymer and monomer segments are accounted for by the Flory χ parameter.

Next consider the surface term. Assuming that the interaction between the polymer segments and the adsorbed layer of surfactants is repulsive, the surface term represents the effect of the depletion of polymer segments near the surfactant layer, which in the emulsion polymerization literature is also known as the "repulsive wall" effect. It is commonly accepted[19] that for polymer particles produced by emulsion polymerization the repulsive wall effect does not produce a significantly nonuniform monomer distribution. Careful small-angle X-ray scattering experiments[29] have shown that the width of the depletion zone is only a few nanometers and is negligible compared to the size of the particles. While the polymer particles produced by microemulsion polymerization are much smaller than those produced by emulsion polymerization, they are still large compared to the width of the depletion layer. Thus, neglect of the effect of a nonuniform monomer concentration profile on the microemulsion polymerization kinetics is justified. The repulsive wall effect also affects monomer partitioning via the surface contribution $\mu_{mon}^{(part,s)}$ to the monomer chemical potential. However, since the volume of the depletion layer is small compared to the total particle volume, this effect is again negligible.

3.3. Equilibrium Equation. The swelling equilibrium is therefore determined by solving the equation

$$\mu_{mon}^{(mic)} = \mu_{mon}^{(part,b)} \tag{17}$$

with respect to either the swelling parameter (x) of the micelles or with respect to the monomer volume fraction (ν_{mon}) in the particles, recalling that these two parameters are related by mass balance (eq 8).

For polymer particles produced by emulsion polymerization, it is well-known that the swelling in the presence of excess monomer strongly depends on the particle size. This situation is described by the so-called Morton equation[30] that balances the Flory−Huggins bulk polymer free energy (which favors swelling) against the surface energy of the interface between the polymer particles and the aqueous solvent (that opposes swelling). The surface energy introduces a strong dependence of the swelling on the particle size. However, the swelling of the polymer particles during microemulsion polymerization according to eq 18 is completely independent of the particle size. The remarkable difference between the two cases is due to the fact that the surface energy does not play a role for monomer partitioning during microemulsion polymerization. This is because, assuming full coverage of the polymer particles with surfactants, the total area of surfactant monolayer of particles and micelles combined remains constant during the polymerization reaction. Therefore, the total surface energy remains constant and does not influence the monomer partitioning. Thus, for emulsion polymer particles in the presence of excess monomer, swelling is opposed by the particle surface energy. In contrast, for the microemulsion case the swelling of the polymer particles is opposed by the curvature energy of the surfactant micelles. The latter favors swelling of the surfactant micelles with monomer up to their preferred size, which is set by the spontaneous curvature of the surfactant monolayer.

4. Monomer Partitioning from Small-Angle Neutron Scattering

The previous section outlines a theoretical analysis that can only be tested by direct measurement of the size of microemulsion droplets and polymer particles. Previously we have reported the first step toward this goal, namely the results of online SANS spectra of polymerizing C_6MA in mixed DTAB/DDAB microemulsions.[16] However, extraction of particle sizes and polydispersities from these spectra involves many parameters and the fits may not be unique. A better approach exploits the fact that, during the polymerization reaction, only the number density of polymer particles increases, while the unswollen particle size distribution change very little. This is verified experimentally[17,31] and follows from our model[13] for the evolution of the particle size distribution during microemulsion polymerization. Then, if monomer partitioning is governed by equilibrium thermodynamics, the polymerizing microemulsions can be simulated using equilibrium mixtures of fully polymerized microemulsions and their unpolymerized counterparts. The arguments developed in the previous section show that to a first approximation the monomer partitioning is independent of the particle size distribution. Therefore, any small differences that do exist between the particle size distributions of the actual polymerizing microemulsions and the equilibrium mixtures that simulate them should not cause significant differences in the monomer partitioning.

A polymerizing microemulsion at a certain fractional conversion (f) can thus be simulated by an equilibrium mixture for which the weight fraction of fully polymerized microemulsion equals f. Consider the SANS spectra of a series of equilibrium mixtures for different values of f. A great reduction in the number of adjustable parameters comes about since the unswollen particle size and polydispersity are adjustable parameters that are shared by the entire set of spectra, rather than having to be adjusted for each spectrum.

At the low q values over which the SANS spectra are analyzed, the aqueous solution of monomer-swollen micelles exhibits no structure. Furthermore, the volume fraction of monomer swollen polymer particles is very low, especially at lower values of f. Hence, the low q scattering is dominated by the form factor of the monomer-swollen polymer particles. The presence of swollen micelles only leads to a correction in the effective scattering length density of the solvent. Although corrections due to particle−particle interactions are expected to be small, we nevertheless accounted for them in an approximate way, using the analytical equations of Vrij[32] for the absolute scattering intensity from a multicomponent mixture of hard spheres. This is expected to be a reasonable approximation since the thickness of the electric double layers as calculated from the cmc of the surfactant at 60 °C is only about 2 nm, which is much smaller than the typical radius of the polymer particles. Indeed, if we assume that the particles interact via a hard-sphere radius 5 nm larger than their actual size, only a ∼5% decrease in the fitted values of ν_{mon} was observed. The presence of micelles may cause an attractive contribution to the effective particle−particle interaction via a depletion mechanism.[33,34] However, the total effective particle−particle interaction presumably remains repulsive since the latexes are very stable.

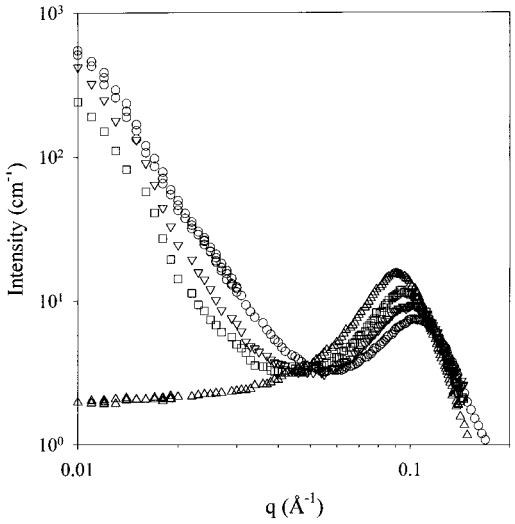

Figure 1. Online SANS spectra $I(q)$ as a function of q for a polymerizing styrene/DTAB/D_2O microemulsion at 60 °C for varying conversions: △, 0%; □, 27%; ▽, 53%; ○, 91%. The initial microemulsion had a composition of $\alpha = 3\%$ and $\gamma = 12\%$.

5. Results and Discussion

An indirect test of whether the results obtained from the equilibrium SANS experiments accurately represent the true partitioning of monomer during microemulsion polymerization is provided by comparing the SANS spectra of the equilibrium mixtures with the corresponding online spectra for polymerizing microemulsions. Online SANS experiments were therefore performed on polymerizing styrene, nC_4MA, tC_4MA, and C_6MA microemulsions at 60 °C. The online SANS spectra for styrene are shown in Figure 1. Spectra for the other monomers were very similar to those for styrene. All sets of spectra display a structure factor peak due to the micelles at intermediate q and intense form factor scattering at low q due to the polymer particles. As the reaction proceeds, the micelle structure factor peak shifts to larger q values, and the particle scattering at low q increases strongly. Very similar trends were observed in our earlier online scattering study on polymerizing C_6MA/DTAB/DDAB/D_2O microemulsions.[16]

Polymerization does not change the electrostatic interactions between the micelles nor does it appreciably change the interfacial area of the micelles since only a small fraction of the total amount of surfactant adsorbs on the polymer particles. Therefore, the progressive decrease in the intermicellar distance, as indicated by the gradual shift in the micelle peak toward higher q, must be due to an increase in micelle number density accompanied by a gradual decrease in micelle size. This qualitative analysis immediately refutes the prediction of the monomer partitioning model of Guo et al.[17] for styrene microemulsion polymerization. That model predicts that the micelles are very quickly depleted of monomer early on in the reaction. In such a scenario, a sudden shift in the micelle peak would have been observed at low conversions.

Figure 2 shows a comparison of the equilibrium SANS spectra with the corresponding online SANS spectra for styrene. The excellent agreement between the two types of SANS spectra was observed for all the other monomers. This agreement validates the approach of simu-

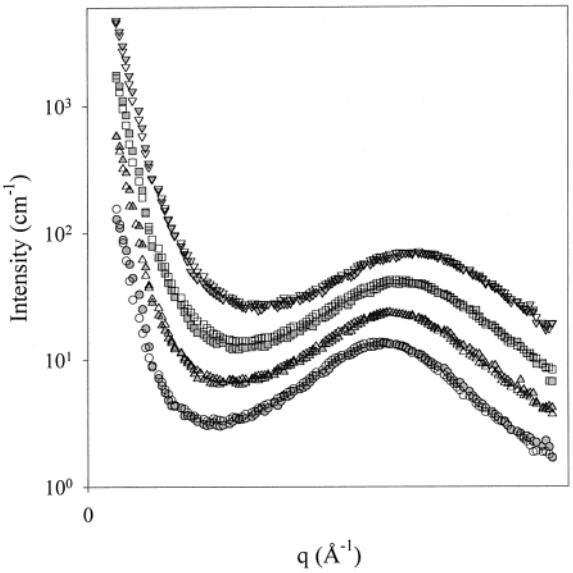

Figure 2. Comparison between SANS spectra obtained online (filled symbols) and obtained from equilibriated mixtures (open symbols) of fully polymerized and unpolymerized styrene/DTAB/D_2O microemulsions at varying conversions: ○, 13%; △, 27%; □, 42%; ▽, 70%. The 27%, 42%, and 70% conversion spectra are offset by factors of 2, 4, and 8, respectively. The initial microemulsion had a composition of $\alpha = 3\%$ and $\gamma = 12\%$.

lating polymerizing microemulsions with equilibriated mixtures of fully polymerized and unpolymerized microemulsions. The agreement between the equilibrium and online SANS spectra extends to much lower q than one may initially expect. This indicates that the size distribution of the polymer particles does indeed remain approximately constant as the polymerization proceeds, consistent with our theory[13] for the evolution of the particle size distribution during microemulsion polymerization. Only at very low conversions (a few percent) are there significant deviations at the lowest q values for the methacrylates. This is obviously due to the fact that, very early in the reaction, the particles have not yet had the time to grow to their ultimate size.

Next we turn to the main part of our results, which are the measurements of monomer partitioning in equilibrium mixtures. Extensive scattering experiments were performed on mixtures of unpolymerized and polymerized microemulsions for styrene, nC_4MA, tC_4MA, and C_6MA. As a representative example, Figure 3 shows the low-q region of the SANS spectra acquired for equilibriated mixtures of fully polymerized and unpolymerized C_6MA microemulsions for various values of f. The lines in these figures represent the fitted SANS model calculations. These fits are obtained by assuming that the unswollen latex size distribution in the mixtures are identical to that in the fully polymerized microemulsion and can be characterized by a Schultz distribution. The Schultz distribution is normalized such that the total volume of polymer is conserved and is then discretized into 10 radii for purposes of calculation. The number densities of the discretized unswollen particle radii are scaled proportionally to the conversion and depend directly on the mixing ratio of the fully polymerized to unpolymerized microemulsion. The volumes and scattering length densities of the discretized unswollen particle radii are also scaled with respect to the volume fraction of monomer in the polymer particles at each level of conversion. The form factor for each

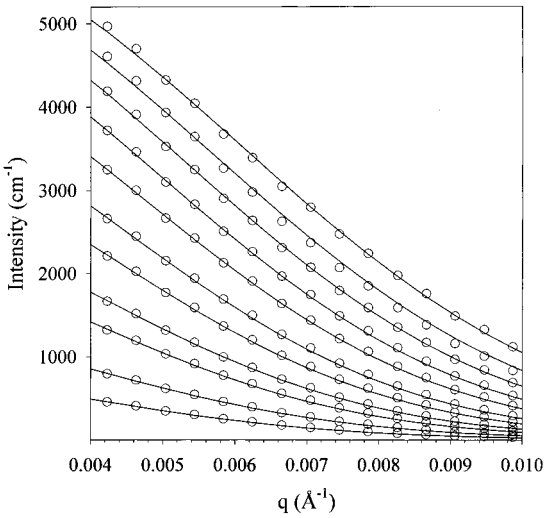

Figure 3. Low-q SANS spectra for mixtures of fully polymerized and unpolymerized nC_6MA/DTAB/D_2O microemulsions for varying mixing ratios. The initial microemulsion had a composition of $\alpha = 3\%$ and $\gamma = 12\%$. From top to bottom, the values of the simulated conversion are 100%, 75%, 55%, 40%, 30%, 20%, 15%, 10%, 7%, 4%, and 2%, respectively. The curves are model scattering spectra calculated as described in section 5.

Table 1. Unswollen Particle Sizes $R_{part,0}$ and Polydispersities $\sigma_{part,0}$ As Determined from Analysis of the SANS Spectra of Mixtures of Fully Polymerized and Unpolymerized Microemulsions; Parameters $\nu_{mon,0}$ and b Were Determined by Fitting the Monomer Partitioning Results to the Interpolation Formula (Eq 18)

monomer	α (%)	$R_{part,0}$ (nm)	$\sigma_{part,0}$ (nm)	$\nu_{mon,0}$ (%)	b
C_6MA	3.0	23	5.2	59	1.4
nC_4MA	3.0	18	4.8	43	1.4
tC_4MA	3.0	13	4.4	43	1.4
styrene	3.0	15	4.7	34	1.0
styrene	5.0	19	5.2	55	1.4
styrene	7.5	19	5.2	69	1.4

particle radii is calculated as described previously,[16] assuming bulk monomer and polymer densities. The volume fraction of monomer in the polymer particles (ν_{mon}) is then used as a single adjustable parameter to fit each of the SANS spectra. Two additional global parameters, the average radius $R_{part,0}$ and standard deviation $\sigma_{part,0}$ of the Schultz distributed unswollen particles, are obtained by simultaneously fitting all of the spectra measured at varying levels of conversion. The spectra of the equilibrium mixtures for the other monomers were analyzed in the same way. The fitted values for $R_{part,0}$ and $\sigma_{part,0}$ for the fully polymerized microemulsions are given in Table 1. As shown in part 3, the fitted Schultz distribution for the unswollen particle size distribution is also in excellent agreement with cryo-TEM measurements. Values for ν_{mon} can be converted into values for the monomer concentration in the particles ($C_{mon}^{(part)}$) by multiplication with the concentration (C_{mon}) of pure monomer that are 8.3 M for styrene, 6.25 M for both butyl methacrylates, and 5.0 M for C_6MA.

The measurements of monomer volume fraction in the particles as a function of conversion for the alkyl methacrylates are collected in Figure 4. The monomer partitioning profiles for the nC_4MA and tC_4MA microemulsions are nearly identical. This is not surprising, considering that the phase behavior of these monomers

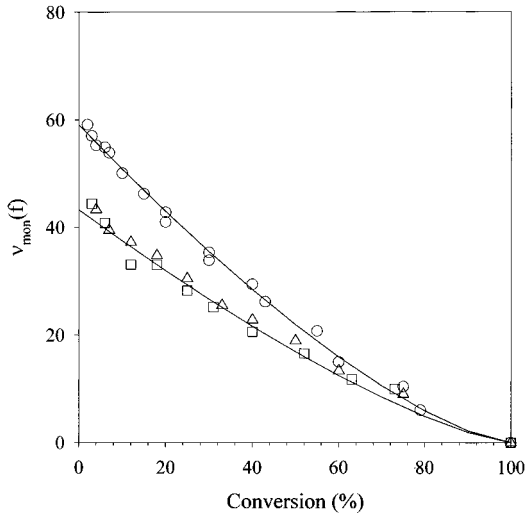

Figure 4. Monomer volume fraction (ν_{mon}) in the polymer particles as a function of conversion as determined from the SANS equilibrium swelling experiments for DTAB/D_2O microemulsions: ○, C_6MA; △, nC_4MA; □, tC_4MA. The initial microemulsion had a composition of $\alpha = 3\%$ and $\gamma = 12\%$. The curves are fits to the empirical interpolation formula (eq 18) with values of the constants $\nu_{mon,0}$ and b as given in Table 1.

are also similar. The initial hypothesis of a linear monomer partitioning profile at least qualitatively describes the data, while deviations from linearity are captured by the following empirical formula:

$$\nu_{mon} = \nu_{mon,0}(1 - f)^b \qquad (18)$$

The value of $\nu_{mon,0}$ represents the extent of swelling of the polymer particles, whereas the value of b represents the shape of the monomer partitioning profile with $b = 1$ corresponding to linear monomer partitioning (eq 1). The lines in Figure 4 correspond to fits to eq 18 for values of the constants $\nu_{mon,0}$ and b as given in Table 1. The fitted value of $b = 1.4$ is not too far off from the value of $b = 1$ for linear monomer partitioning. The values of $\nu_{mon,0}$ for the C_4MA monomers, $\nu_{mon,0} = 43\%$, and for C_6MA, $\nu_{mon,0} = 59\%$, indicate that there is considerable swelling of the polymer particles by the monomer.

Next we consider styrene microemulsion polymerization. At the same weight fraction of surfactant, DTAB solubilizes styrene to a much larger extent than it does C_6MA or the butyl methacrylate monomers. Therefore, for styrene microemulsion polymerization at constant surfactant concentration, the monomer partitioning experiments can be performed over a wider range of monomer concentrations. This allows direct probing of the influence of microemulsion composition on monomer partitioning. Equilibrium SANS experiments were performed for microemulsions containing $\alpha = 3\%$, 5%, and 7.5% monomer at a surfactant weight fraction of $\gamma = 12\%$. Figure 5 shows the sample locations in the styrene/DTAB/D_2O phase diagram at 60 °C. The monomer partitioning results are shown in Figure 6. The $\alpha = 3\%$ data were obtained from repeat measurements of samples made from two separately prepared latexes and hence give an indication of the overall measurement precision. Again, the lines are fits to eq 18, for values of the constants $\nu_{mon,0}$ and b as given in Table 1.

In agreement with the results of Manders et al.,[18] the monomer volume fraction in the polymer particles at low conversion increases strongly with increasing monomer content of the initial microemulsion. Remarkably, at low monomer content, $\alpha = 3\%$, the styrene monomer partitioning is almost perfectly linear. Moving closer to the phase boundary, for $\alpha = 5\%$ and 7.5%, the monomer partitioning again becomes more nonlinear, with $b \approx 1.4$.

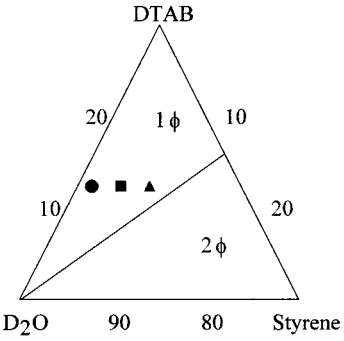

Figure 5. Schematic partial ternary phase diagram for styrene/DTAB/D_2O at 60 °C. The compositions used in the equilibrium swelling experiments are indicated by the symbols, which are the same as in Figure 6. The one- and two-phase regions are denoted by 1ϕ and 2ϕ, respectively.

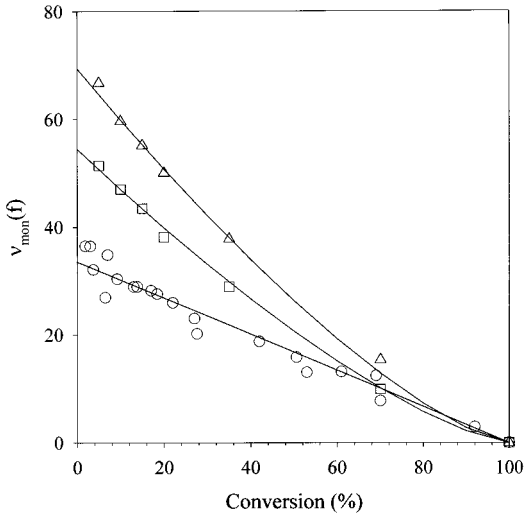

Figure 6. Monomer volume fraction (ν_{mon}) in the polymer particles as a function of conversion as determined from the SANS equilibrium swelling experiments for styrene/DTAB/D_2O microemulsions. The initial microemulsion had compositions of $\gamma = 12\%$ DTAB and (○) $\alpha = 3\%$, (□) $\alpha = 5\%$, and (△) $\alpha = 7.5\%$. The full curves are fits to the empirical interpolation formula (eq 18) with values of the constants $\nu_{mon,0}$ and b as given in Table 1.

Next the predictions of the thermodynamic monomer partitioning model (section 3) are compared to the experimental monomer partitioning results for styrene. It is well-known that the Flory χ parameter characterizing the polymer−monomer interaction as determined experimentally may be a strong function of the polymer volume fraction.[35] The volume fractions of polymer in the monomer swollen polymer particles are in fact comparable to those encountered in emulsion polymerization. As an estimate for the χ parameter for polystyrene in styrene, we therefore take $\chi = 0.26$ as found from vapor pressure measurements on polystyrene latexes swollen with styrene at 60 °C.[36] Using $R_{mic,0} = 1.5$ nm for the radius of the empty DTAB micelles, the only remaining adjustable parameter in the comparison with the experimental results is the combination of elastic constants ($k_c c_0$) of the surfactant monolayers that

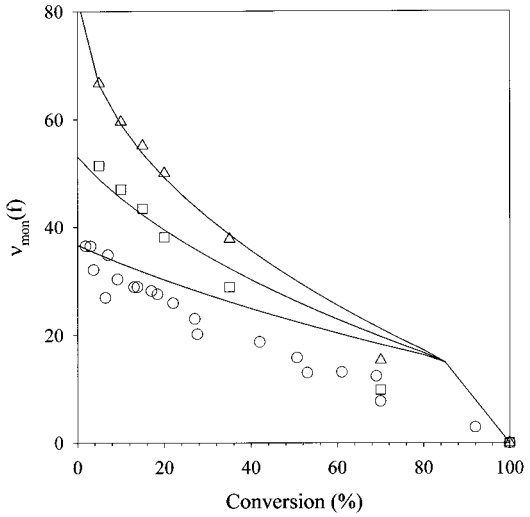

Figure 7. Comparison of SANS equilibrium swelling results for styrene/DTAB/D_2O microemulsions with calculations from the thermodynamic model of section 3 for (○) $\alpha = 3\%$, (□) $\alpha = 5\%$, and (△) $\alpha = 7.5\%$. The parameter values that were used to calculate the theoretical curve are the measured values of $R_{mic,0} = 1.5$ nm and $\chi = 0.26$ and the fitted value of $k_c c_0 = 2.4 k_B T$ nm^{-1}, as well as the experimentally determined location of the phase boundary at $\alpha = 8.2$ wt %.

characterizes the micelle−monomer interaction. Figure 7 compares the predictions of the thermodynamic model with the experimental results for styrene. The fitted value of the surfactant monolayer elastic constant is $k_c c_0 = 2.4 k_B T$ nm^{-1}. While this is larger than some reported values,[37,38] it is still within the physically reasonable range, especially considering that the maximum droplet sizes are quite small for styrene/DTAB microemulsions. Furthermore, since these microemulsions do not contain any added electrolyte, there will be a significant contribution to the elastic constants due to the electric double layers.[22−25]

At low conversions, the theory accurately predicts the initial volume fraction of monomer in the particles as a function of the total weight fraction of monomer in the unpolymerized microemulsions. The theory also captures the increasingly nonlinear monomer partitioning profiles close to the phase boundary. At higher conversions, the theory overestimates the monomer volume fraction in the polymer particles. Beyond the break in the theoretical curves at $\nu_{mon} \approx 80\%$, the theory predicts that monomer partitions exclusively into the particles, and no monomer remains in the micelles. Hence, beyond the break, all curves coincide and are given by $\nu_{mon} = 1 - f$. This is clearly an artifact of the mean-field approximation used in our theory. In reality, there will always be some monomer in the micelles due to various kinds of fluctuations that were not taken into account, such as the size and shape fluctuations of the monomer-swollen micelles.

Finally, we have unfortunately not been able to measure the monomer partitioning for C_6MA microemulsion polymerizations with mixed DTAB and DDAB surfactants. Although the latex particles are highly stable when polymerized in H_2O, noticeable creaming occurs in the corresponding D_2O latexes within 15−30 min. Thus, we have not been able to carry out reproducible equilibrium SANS experiments using the protocols developed here. However, the present work does provide a detailed a posteriori justification for our previous ad hoc assumptions of linear monomer partitioning and limited particle swelling for that system. The DTAB micelles solubilize only small amounts of C_6MA while, at a surfactant weight fraction of $\gamma = 12\%$ and a monomer weight fraction of $\alpha = 3\%$, the C_6MA/DTAB microemulsions are in fact close to their phase boundary ($\alpha = 3.2\%$). This explains our observations of strong particle swelling and significantly nonlinear monomer partitioning for these microemulsions. On the other hand, the mixed DTAB/DDAB micelles solubilize C_6MA to a much larger extent with the phase boundary lying at $\alpha = 7.5\%$. Therefore, at the same weight fraction of surfactant and monomer, the mixed microemulsions are much farther away from their phase boundary. In view of our findings for styrene and in view of the predictions of the thermodynamic model, we expect that for the mixed microemulsions monomer partitioning should be indeed be linear and particle swelling should be limited, as was assumed.

6. Conclusions

Both experiment and theory show that monomer partitioning during microemulsion polymerization strongly depends on the microemulsion composition, especially on the distance to the phase boundary. If the composition of the initial microemulsion is far away from the phase boundary, monomer partitioning is essentially linear, and the monomer concentration in the polymer particles is low. For initial microemulsion compositions close to the phase boundary, monomer partitioning is significantly nonlinear, and the monomer concentration in the particles is much higher. These results can be directly used in theories for the kinetics of microemulsion polymerization.

Acknowledgment. We are grateful for the financial support of Uniqema and acknowledge the support of the National Institute of Standards and Technology, U.S. Department of Commerce, for providing the neutron research facilities used in this work. This work is also supported by the Netherlands Foundation for Scientific Research (NWO) and the National Science and Engineering Research Council of Canada.

References and Notes

(1) Rabelero, M.; Zacarias, M.; Mendizabal, E.; Puig, J. E.; Dominguez, J. M.; Katime, I. *Polym. Bull.* **1997**, *38*, 695.
(2) Ming, W. H.; Jones, F. N.; Fu, S. K. *Polym. Bull.* **1998**, *40*, 749.
(3) Morgan, J. D.; Johnson, C. A.; Kaler, E. W. *Langmuir* **1997**, *13*, 6447.
(4) Desai, S. D.; Gordon, R. D.; Gronda, A. M.; Cussler, E. L. *Curr. Opin.* **1996**, *1*, 519.
(5) Meier, W. *Curr. Opin. Colloid Interface Sci.* **1999**, *4*, 6.
(6) Candau, F. Polymerization in Microemulsions. In *Polymerization in Organized Media*; Paleos, C. M., Ed.; Gordon and Breach Science Publishers: Philadelphia, 1992; p 215.
(7) Antonietti, M.; Baster, R.; Lohmann, S. *Macromol. Chem. Phys.* **1995**, *196*, 441.
(8) Guo, J. S.; Sudol, E. D.; Vanderhoff, J. W.; El-Aasser, M. S. *J. Polym. Sci., Polym. Chem.* **1992**, *30*, 703.
(9) Mendizabal, E.; Flores, J.; Puig, J. E.; Lopez-Serrano, F.; Alvarez, J. *Eur. Polym. J.* **1998**, *34*, 411.
(10) Morgan, J. D.; Lusvardi, K. M.; Kaler, E. W. *Macromolecules* **1997**, *30*, 1897.
(11) Nomura, M.; Suzuki, K. *Macromol. Chem. Phys.* **1997**, *198*, 3025.
(12) Suzuki, K.; Nomura, M.; Harada, M. *Colloids Surf. A* **1999**, *153*, 23.
(13) Morgan, J. D.; Kaler, E. W. *Macromolecules* **1998**, *31*, 3197.
(14) Capek, I.; Juranicova, V. *Eur. Polym. J.* **1998**, *34*, 783.
(15) Full, A. P.; Puig, J. E.; Gron, L. U.; Kaler, E. W.; Minter, J. R.; Mourey, T. H.; Texter, J. *Macromolecules* **1992**, *25*, 5157.

(16) Co, C. C.; Kaler, E. W. *Macromolecules* **1998**, *31*, 3203.
(17) Guo, J. S.; Sudol, E. D.; Vanderhoff, J. W.; El-Aasser, M. S. *J. Polym. Sci., Polym. Chem. Ed.* **1992**, *30*, 691.
(18) Manders, B. G.; van Herk, A. M.; German, A. L. *Makromol. Chem., Rapid Commun.* **1993**, *14*, 693.
(19) Gilbert, R. G. *Emulsion Polymerization: A Mechanistic Approach*; Academic Press: San Diego, 1995.
(20) Helfrich, W. *Z. Naturforsch.* **1973**, *28C*, 693.
(21) *Micellees, Membranes, Microemulsions and Monolayers*; Springer: New York, 1994.
(22) Winterhalter, M.; Helfrich, W. *J. Phys. Chem.* **1988**, *92*, 6865.
(23) Mitchell, D. J.; Ninham, B. W. *Langmuir* **1989**, *5*, 1121.
(24) Lekkerkerker, H. N. W. *Physica A* **1989**, *159*, 319.
(25) Lekkerkerker, H. N. W. *Physica A* **1990**, *167*, 384.
(26) Palmer, K. M.; Morse, D. C. *J. Chem. Phys.* **1996**, *105*, 11147.
(27) Kegel, W. K.; Reiss, H. *Ber. Bunsen-Ges. Phys. Chem.* **1996**, *100*, 300.
(28) Kegel, W. K.; Reiss, H. *Ber. Bunsen-Ges. Phys. Chem.* **1997**, *101*, 1963.
(29) Bolze, J.; Ballauff, M. *Macromolecules* **1995**, *28*, 7429.
(30) Morton, M.; Kaizerman, S.; Altier, M. W. *J. Colloid Sci.* **1954**, *9*, 301.
(31) Bleger, F.; Murthy, A. K.; Pla, F.; Kaler, E. W. *Macromolecules* **1994**, *27*, 2559.
(32) Vrij, A. *J. Chem. Phys.* **1979**, *71*, 3267.
(33) Kline, S. R.; Kaler, E. W. *Langmuir* **1996**, *12*, 2402.
(34) Kline, S. R.; Kaler, E. W. *J. Chem. Phys.* **1996**, *105*, 3813.
(35) *Polymer Handbook*, 3rd ed.; Brandrup, J., Immergut, E. H., Eds.; John Wiley & Sons: New York, 1989.
(36) Vanzo, E.; Marchessault, R. H.; Stannett, V. *J. Colloid Sci.* **1965**, *20*, 62.
(37) Kegel, W. K.; Bodnar, I.; Lekkerkerker, H. N. W. *J. Phys. Chem.* **1995**, *99*, 3272.
(38) Kellay, H.; Meunier, J.; Binks, B. P. *Phys. Rev. Lett.* **1993**, *70*, 1485.

MA001246R